Progress In Electromagnetics Research, PIER 47, 263–296, 2004

REFLECTION AND TRANSMISSION FROM A THIN INHOMOGENEOUS CYLINDER IN A RECTANGULAR TE_{10} WAVEGUIDE

M. R. Booty and G. A. Kriegsmann

Department of Mathematical Sciences
New Jersey Institute of Technology
University Heights, Newark, New Jersey 07102-1982, USA

Abstract—We study the scattering problem for a thin cylindrical target that is placed with arbitrary orientation in a rectangular TE_{10} waveguide and subjected to an imposed electromagnetic field. The scattered far-field is expressed in terms of the scattered field inside the target and the far-field expansion of the dyadic Green's function for the waveguide. In order to capture features of interest in microwave heating applications, we allow the target material's electrical properties to be arbitrary functions of position along the thin cylindrical target's axis. Reflection and transmission coefficients for such a target, and an expression for the rate of deposition of electromagnetic energy within it are derived.

1. INTRODUCTION

We consider the scattered field due to a thin cylindrical target of circular cross-section that is subject to an imposed electromagnetic field in a TE_{10} waveguide. The cylinder has small aspect ratio, i.e., its average radius is much less than the waveguide width, its permittivity and electrical conductivity are allowed to be arbitrary functions of distance along its axis, and the axis can have arbitrary orientation relative to the direction of the imposed field within the waveguide. The cylinder radius may also vary on the length scale of the waveguide width.

Two motives for determining the scattered field are: (i) Expressions for the reflection and transmission coefficients that result from the analysis allow the electrical properties of a material to be determined by irradiating a sample of it with a known field and measuring the reflected and transmitted fields. (ii) In microwave heating and similar applications, it is desirable to predict features such as the rate of heating and temperature distribution for a target sample of known properties. This requires determination of the total electromagnetic field experienced by the target at each point, and thereby depends on solving the problem for the scattered field.

Approximate and variational formulas for scattering from a thin cylinder in a waveguide have been derived before. A survey of classical techniques and results is given in [1] and more recent studies based on mode-matching methods have appeared in, for example, references [2] to [6]. Some of these results are for a cylinder that is perfectly conducting and others are for a more general lossy dielectric target, but in all cases the electrical properties are taken to be constant in the direction along the cylinder's axis and the axis has a specific orientation that is either parallel or perpendicular to the irradiating field. The method we use to construct the scattered field is similar to that of [7], in which charge and current distributions on the target surface are introduced and satisfy an integral equation which is then solved by an iterative procedure based on the target's small aspect ratio. Here we replace solution of the integral equation with solution of the boundary value problem for the scattered near-field based on the method of multiple scales [8].

Both of the motives we have in mind are relevant to the behavior of materials such as ceramics when subject to an electromagnetic field

of microwave frequency. In almost all cases, the electrical conductivity of ceramics increases with frequency and increases more substantially with temperature. Their permittivity also varies, increasing with temperature and, in general, decreasing with frequency. The study of Westphal [9] remains one of the most comprehensive sources of data on the subject. It notes that, for example, the electrical conductivity of alumina (Al_2O_3, of purity 99%) at 4 GHz increases from $5 \times 10^{-6}(\Omega\text{cm})^{-1}$ at 30°C to $6 \times 10^{-4}(\Omega\text{cm})^{-1}$ at 1400°C and the electrical conductivity of silica (SiO_2, of purity 99.97%) at 6 GHz increases from $1.5 \times 10^{-6}(\Omega\text{cm})^{-1}$ at 30°C to $1 \times 10^{-4}(\Omega\text{cm})^{-1}$ at 1200°C. Most high-temperature data of the study were found using a microwave cavity, and it is noted that impurities tend to substantially increase a ceramic's electrical conductivity.

Our motive for generalizing to a target that has spatially inhomogeneous electrical properties arises primarily from applications such as microwave heating where the intensity of the irradiating field is not small. If the material that the target consists of is spatially homogeneous, i.e., has uniform chemical structure throughout the target volume, then the target's electrical properties, its permittivity and conductivity, are spatially uniform throughout its volume unless, as may occur in practice, the target sustains a temperature gradient and the material's electrical properties are temperature-dependent.

When the amplitude of the imposed field is small, the dipolar and Ohmic heating that the imposed field induces in the material is also small and the target is close to a uniform, ambient temperature. That is, the coupling from the electromagnetic to the thermodynamic field is weak, and any coupling from the thermodynamic field to the electromagnetic field is so small that it can be neglected in a first approximation. However, this may change as the amplitude of the imposed field increases.

In general, since both the imposed electromagnetic field in the waveguide and the total field in the presence of the target have non-zero spatial gradients, there is a spatial gradient in the power deposition or rate of generation of heat within the target. For an imposed field of sufficiently large amplitude and a target material of finite or small thermal conductivity, this causes a spatial gradient in the target's temperature. If the target material's electrical properties are temperature-dependent there is then a mutual coupling of the electromagnetic and thermodynamic fields. The target's temperature gradient influences both the scattered part of the electromagnetic field and the rate of heat generation within it via gradients or inhomogeneities in its electrical properties.

When the target has small aspect ratio, the variation in

temperature across its narrow cross-section is small, while the variation across its greater cross-section is not small. For a thin cylindrical target, we therefore allow its electrical properties to be arbitrary functions of distance in the axial direction while being constant in the radial direction. Quantitative justification for this model of the electrical properties' distribution has been given in the context of the microwave heating of a thin cylinder in the small Biot number limit in [10] and [11].

The amplitude of the scattered electric field depends on the target material's electrical properties through the single dimensionless quantity $N^2 = \epsilon/\epsilon_0 + i\sigma/\omega\epsilon_0$ where ϵ is the material's permittivity and ϵ_0 is the permittivity of free space, σ is the material's effective electrical conductivity, and ω is the angular frequency of the imposed field, which has frequency 2.45 GHz in standard microwave applications. The analysis we present is for the case where $\mathrm{Im}(N^2)$ is of order one or small. For values of $\mathrm{Im}(N^2)$ that are large, which occur for materials with large electrical conductivity, the analysis begins to fail, since the material expels the imposed field across a narrow boundary layer or skin with depth of the order $\delta = c_0\sqrt{2\epsilon_0/\omega\sigma}$, [12] which is not included in our analysis. However, microwaves do not provide an effective means of heating a material with large electrical conductivity, and other methods can provide a more suitable means of determining its electrical properties.

The structure of the paper is as follows. In Section 2, we formulate the imposed field for a TE_{10} waveguide, with or without a conducting short. In Section 3, we construct a representation for the scattered electric field far from the target (i.e., the scattered far-field) in terms of an integral taken over the target volume of the total electric field and the far-field expansion of the dyadic Green's function for the waveguide. At the end of Section 3 we give the far-field representation of the dyadic Green's function in terms of left and right-going TE_{10} waves within the guide, while construction of the Green's function is given in the Appendix. To find the total field within the target, we construct the scattered field both in and near the target (i.e., the scattered near-field) in Section 4 by appealing to the target's small aspect ratio and introducing a multiple scale perturbation method [8]. At the end of Section 4 we compute an expression for the rate at which the electromagnetic field deposits energy within the target. The target's reflection and transmission coefficients are given in Section 5, where an identity based on conservation of energy is used as a partial check on the expressions that are found, and examples for specific target orientation and electrical properties are given.

2. FORMULATION

We consider a thin cylindrical target placed in a TE_{10} waveguide. The waveguide's axis is in the z-direction and its cross-section is rectangular with $x \in [0,\, W]$ and $y \in [0,\, H]$. The electric and magnetic fields $\boldsymbol{E}$ and $\boldsymbol{H}$ are time-harmonic with time-dependence $e^{-i\omega t}$, so that in complex form a right-going TE_{10} wave with amplitude E_0 incident from $z = -\infty$ has electric field

$$\boldsymbol{E} = E_0 \sin \frac{\pi x}{W} e^{ik_{10}z} \boldsymbol{e}^{(2)} \tag{1}$$

where $k_{10} = \sqrt{k^2 - \frac{\pi^2}{W^2}}$, $k = \omega/c_0$ is the free space wave number, and $\boldsymbol{e}^{(i)}$ is a unit vector in the direction of the i^{th} Cartesian coordinate axis.

In the absence of a short (1) is the electric field imposed on the target. If the waveguide is equipped with a perfectly conducting short at $z = L$ then the imposed field consists of the sum of the same right-going TE_{10} wave and a superimposed left-going TE_{10} wave which together satisfy the boundary condition of zero tangential electric field on the short. The imposed field is written as

$$\boldsymbol{E}_i = E_i \boldsymbol{e}^{(2)}, \tag{2}$$

where, on factoring its amplitude E_0,

$$E_i = E_0 e_i \quad \text{and} \quad e_i = \sin \frac{\pi x}{W} \begin{cases} e^{ik_{10}z} & \text{no short} \\ e^{ik_{10}z} - e^{-ik_{10}(z-2L)} & \text{with short.} \end{cases} \tag{3}$$

The waveguide geometry and a typical orientation for the target are shown in Figure 1.

In the near-field of the cylindrical target, i.e., inside and near it, the scattered part of the electromagnetic field varies in the transverse plane perpendicular to the cylinder axis on the length scale of the cylinder's radius, or on its average value ρ_0. However, in the axial direction of the cylinder it varies on the length scale of the imposed field and waveguide width W. Since the cylinder's aspect ratio $\alpha = \rho_0/W$ is small, these two spatial scales are greatly separated; the construction of the near-field in Section 4 makes explicit use of this separation of spatial scales.

The small-scale structure of the near-field decays with increasing distance away from the cylinder axis, and it then varies on the single scale W. Here the electromagnetic field has an expansion in terms

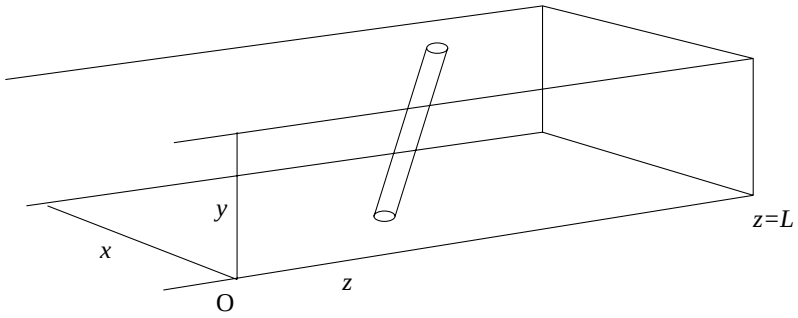

Figure 1. Coordinate system for a TE_{10} waveguide with short and a typical orientation for the cylindrical target. The cylinder's radius is small compared to the waveguide width.

of the eigenfunctions of the waveguide, but with further increase in distance away from the target, since all eigenfunctions in a TE_{10} guide are evanescent except for that of the propagating TE_{10} wave, the scattered far-field signal can be expressed in terms of TE_{10} waves alone, with amplitude to be found.

3. REPRESENTATION OF THE SCATTERED FIELD IN TERMS OF THE DYADIC GREEN'S FUNCTION

Both inside and outside the target, the curl equations are

$$\begin{aligned} \nabla \wedge \boldsymbol{E} &= i\omega\mu_0 \boldsymbol{H} \\ \nabla \wedge \boldsymbol{H} &= -i\omega\epsilon_0 N^2 \boldsymbol{E}. \end{aligned} \tag{4}$$

The second equation pertains to a medium with permittivity ϵ and current density $\boldsymbol{j}$ given by Ohm's law $\boldsymbol{j} = \sigma \boldsymbol{E}$ where σ is an effective electric conductivity, for which $\nabla \wedge \boldsymbol{H} = (\sigma - i\omega\epsilon)\boldsymbol{E}$. Thus

$$N^2 = \frac{\epsilon}{\epsilon_0} + i\frac{\sigma}{w\epsilon_0}. \tag{5}$$

N^2 is the one grouping of the material's electrical properties ϵ and σ that will appear. It is dimensionless and of order one, and is discontinuous across the target surface. Everywhere outside the target $N^2 = 1$; inside the target, for the purposes of this section it can be an arbitrary function of position, while for our model of a thin cylindrical target it is a function of the axial coordinate alone.

The electric and magnetic fields are decomposed as the sum of imposed fields $(\boldsymbol{E}_i, \boldsymbol{H}_i)$ which persist throughout the waveguide in the absence of the target and scattered fields $(\boldsymbol{E}_s, \boldsymbol{H}_s)$ due to the presence of the target. That is

$$\boldsymbol{E} = \boldsymbol{E}_i + \boldsymbol{E}_s \quad \text{and} \quad \boldsymbol{H} = \boldsymbol{H}_i + \boldsymbol{H}_s, \tag{6}$$

where the imposed fields satisfy the curl equations

$$\begin{aligned} \nabla \wedge \boldsymbol{E}_i &= i\omega\mu_0 \boldsymbol{H}_i \\ \nabla \wedge \boldsymbol{H}_i &= -i\omega\epsilon_0 \boldsymbol{E}_i. \end{aligned} \tag{7}$$

Subtracting equations (7) from equations (4), we find that the scattered fields satisfy

$$\begin{aligned} \nabla \wedge \boldsymbol{E}_s &= i\omega\mu_0 \boldsymbol{H}_s \\ \nabla \wedge \boldsymbol{H}_s &= -i\omega\epsilon_0 N^2 \boldsymbol{E}_s - i\omega\epsilon_0 (N^2 - 1)\boldsymbol{E}_i. \end{aligned} \tag{8}$$

The magnetic field is eliminated from equations (8) on taking the curl of the first equation, to give

$$\nabla \wedge \nabla \wedge \boldsymbol{E}_s = k^2 N^2 \boldsymbol{E}_s + k^2 (N^2 - 1)\boldsymbol{E}_i \tag{9}$$

where $k = \omega / c_0$ is the free space wavenumber.

The electric and magnetic fields of the dyadic Green's function $(\boldsymbol{E}_{Gi}, \boldsymbol{H}_{Gi})$ are due to an isolated point current with strength j_0 that is located at $\boldsymbol{x} = \boldsymbol{x'}$ within the waveguide and is oriented in the direction $\boldsymbol{e}^{(i)}$. They satisfy

$$\begin{aligned} \nabla \wedge \boldsymbol{E}_{Gi} &= i\omega\mu_0 \boldsymbol{H}_{Gi} \\ \nabla \wedge \boldsymbol{H}_{Gi} &= -i\omega\epsilon_0 \boldsymbol{E}_{Gi} + j_0 \delta(\boldsymbol{x} - \boldsymbol{x'})\boldsymbol{e}^{(i)}. \end{aligned} \tag{10}$$

When the curl of the first equation is taken to eliminate the magnetic field, we have

$$\nabla \wedge \nabla \wedge \boldsymbol{E}_{Gi} = k^2 \boldsymbol{E}_{Gi} + i\omega\mu_0 j_0 \delta(\boldsymbol{x} - \boldsymbol{x'})\boldsymbol{e}^{(i)}. \tag{11}$$

Forming the dot product of $\boldsymbol{E}_s$ with equation (11) minus the dot product of $\boldsymbol{E}_{Gi}$ with equation (9) and simplifying the left-hand side using the vector identity $\nabla \cdot (\boldsymbol{a} \wedge \boldsymbol{b}) = \boldsymbol{b} \cdot (\nabla \wedge \boldsymbol{a}) - \boldsymbol{a} \cdot (\nabla \wedge \boldsymbol{b})$, we have

$$\begin{aligned} &\nabla \cdot ((\nabla \wedge \boldsymbol{E}_{Gi}) \wedge \boldsymbol{E}_s - (\nabla \wedge \boldsymbol{E}_s) \wedge \boldsymbol{E}_{Gi})) = \\ &\quad -k^2 (N^2 - 1)\boldsymbol{E} \cdot \boldsymbol{E}_{Gi} + i\omega\mu_0 j_0 \delta(\boldsymbol{x} - \boldsymbol{x'})\boldsymbol{E}_s \cdot \boldsymbol{e}^{(i)}. \end{aligned} \tag{12}$$

This last relation is integrated over (i) a rectangular volume V^+ of the waveguide that is exterior to the target and bounded by the

waveguide sidewalls and planes S_1 and S_2 of constant z to either side of the target, and over (ii) the complementary volume V of the target itself. The results simplify due to the boundary conditions on the waveguide sidewalls and the jump conditions across the target surface. The waveguide sidewalls are perfectly conducting, so that the tangential component of the electric field and the normal derivative of its normal component vanish there. This applies to each of the imposed, scattered, and dyadic Green's function fields separately, that is,

$$\boldsymbol{E}_k \wedge \boldsymbol{n} = 0 \quad \text{and} \quad \frac{\partial}{\partial n}(\boldsymbol{E}_k \cdot \boldsymbol{n}) = 0 \ \text{ on the waveguide sidewalls} \tag{13}$$

for $k = i, s$, and Gi. Since the target conductivity is finite, equations (8) imply that the tangential component of the scattered electric and magnetic fields are continuous across the target surface, which expressed in terms of $\boldsymbol{E}_s$ alone becomes

$$[\boldsymbol{E}_s \wedge \boldsymbol{n}] = 0 \quad \text{and} \quad [(\nabla \wedge \boldsymbol{E}_{\mathrm{s}}) \wedge \boldsymbol{n}] = 0 \tag{14}$$

where $[\cdot]$ denotes the jump across the target surface S.

When equation (12) is integrated over the volume V^+ and $\boldsymbol{x}'$ is inside V^+, where $N^2 = 1$, we find on applying the divergence theorem that

$$\begin{aligned} i\omega\mu_0 j_0 \boldsymbol{E}_s(\boldsymbol{x}') \cdot \boldsymbol{e}^{(i)} = &\int_{S_1+S_2} (\nabla \wedge \boldsymbol{E}_{Gi}) \cdot (\boldsymbol{E}_s \wedge \boldsymbol{n}) - (\nabla \wedge \boldsymbol{E}_s) \cdot (\boldsymbol{E}_{Gi} \wedge \boldsymbol{n}) dS \\ &- \int_{S+} (\nabla \wedge \boldsymbol{E}_{Gi}) \cdot (\boldsymbol{E}_s \wedge \boldsymbol{n}) - (\nabla \wedge \boldsymbol{E}_s) \cdot (\boldsymbol{E}_{Gi} \wedge \boldsymbol{n}) dS. \end{aligned} \tag{15}$$

Here, the unit normal $\boldsymbol{n}$ points outward from the boundary of V^+ except on the target surface S where $\boldsymbol{n}$ points outward from the target, and S^+ denotes that the scattered field $\boldsymbol{E}_s$ and its derivatives, which are discontinuous across S, are evaluated immediately outside S.

In (15) the surface integral over the perfectly conducting waveguide sidewalls is zero and has been omitted, since the boundary conditions (13) imply that the tangential components of $\boldsymbol{E}_s$ and $\boldsymbol{E}_{Gi}$ are zero there. The integrals over the planes S_1 and S_2 also vanish, as is clear when the planes are taken far from $\boldsymbol{x}'$ and the target. To see this, we note that since the waveguide permits only a TE_{10} mode to propagate, in the absence of a short both $\boldsymbol{E}_s$ and $\boldsymbol{E}_{Gi}$ are scalar multiples of a left-going TE_{10} mode on S_1 and are multiples of a right-going TE_{10} mode on S_2. The anti-symmetry of the integrand under interchange of $\boldsymbol{E}_s$ and $\boldsymbol{E}_{Gi}$ implies that the integrand vanishes on each of S_1 and S_2, so that the integrals vanish separately. In the presence

of a perfectly conducting short, S_2 is chosen to coincide with the short and the boundary conditions (13) apply, so that the integrand over S_2 is again zero. Thus, (15) is

$$i\omega\mu_0 j_0 \boldsymbol{E}_s(\boldsymbol{x}')\cdot\boldsymbol{e}^{(i)} = -\int_{S+}(\nabla\wedge\boldsymbol{E}_{Gi})\cdot(\boldsymbol{E}_s\wedge\boldsymbol{n})-(\nabla\wedge\boldsymbol{E}_s)\cdot(\boldsymbol{E}_{Gi}\wedge\boldsymbol{n})dS. \tag{16}$$

Integration of equation (12) over the volume of the target V, gives

$$\int_{S^-}(\nabla\wedge\boldsymbol{E}_{Gi})\cdot(\boldsymbol{E}_s\wedge\boldsymbol{n})-(\nabla\wedge\boldsymbol{E}_s)\cdot(\boldsymbol{E}_{Gi}\wedge\boldsymbol{n})dS + k^2\int_V(N^2-1)\boldsymbol{E}\cdot\boldsymbol{E}_{Gi}dV = 0 \tag{17}$$

where S^- denotes that the scattered field is evaluated immediately inside S. Combining equations (16) and (17), we find that

$$i\omega\mu_0 j_0 \boldsymbol{E}_s(\boldsymbol{x}')\cdot\boldsymbol{e}^{(i)} = -\int_S[(\nabla\wedge\boldsymbol{E}_{Gi})\cdot(\boldsymbol{E}_s\wedge\boldsymbol{n})-(\nabla\wedge\boldsymbol{E}_s)\cdot(\boldsymbol{E}_{Gi}\wedge\boldsymbol{n})]^+_-dS + k^2\int_V(N^2-1)\boldsymbol{E}\cdot\boldsymbol{E}_{Gi}dV$$

where $[\cdot]^+_-$ denotes the jump across the target surface S. In this last expression, the surface integral over S is zero since $\boldsymbol{E}_{Gi}$ is smooth across S while the boundary conditions (14) imply that both $\boldsymbol{E}_s\wedge\boldsymbol{n}$ and $(\nabla\wedge\boldsymbol{E}_s)\wedge\boldsymbol{n}$ are continuous across S. Hence

$$i\omega\mu_0 j_0 \boldsymbol{E}_s(\boldsymbol{x}')\cdot\boldsymbol{e}^{(i)} = k^2\int_V(N^2-1)\boldsymbol{E}\cdot\boldsymbol{E}_{Gi}dV. \tag{18}$$

This gives the scattered field at a point $\boldsymbol{x}'$ outside the target in terms of the total field and dyadic Green's function integrated over the target volume.

When $\boldsymbol{x}'$ is removed far from the target, equation (18) gives the scattered far-field needed for calculation of the target's reflection and transmission coefficients. However, since the scattered far-field in a TE_{10} waveguide consists of propagating TE_{10} waves alone, $\boldsymbol{E}_s$ is in the direction of $\boldsymbol{e}^{(2)}$ with magnitude E_s given by setting $i=2$ in (18). The construction of the dyadic Green's function for the waveguide is given in the Appendix, and since only the y-component of the Green's function contributes to the scattered far-field, its contribution is given by taking the one term with $m=1$ and $n=0$ in the sum of equation (A7) there. This is the far-field approximation of the Green's function (A8), which is written as $\boldsymbol{E}_{G2}\sim E^p_{G2}\boldsymbol{e}^{(2)}$, where

$$E^P_{G2}(\boldsymbol{x},\boldsymbol{x}') =$$

$$\frac{-j_0k^2}{\omega\epsilon_0 WHk_{10}}\sin\frac{\pi x}{W}\sin\frac{\pi x'}{W}\begin{cases} e^{ik_{10}|z-z'|} & \text{no short} \\ e^{ik_{10}|z-z'|}-e^{-ik_{10}(z+z'-2L)} & \text{with short.}\end{cases} \tag{19}$$

Inspection shows that (19) is a scalar multiple of a left-going TE_{10} wave with argument the left-most in the z direction of $\boldsymbol{x}$ or $\boldsymbol{x}'$, multiplied by the scaled imposed field e_i of (3) with argument the right-most of $\boldsymbol{x}$ or $\boldsymbol{x}'$. Like the imposed field, the Green's function varies solely on the length scale of the waveguide width W, so that by the same reasoning given after equation (33) below, when E_{G2} is expressed in terms of polar coordinates in and near the target it is represented by its Taylor series in r, in which the magnitude of successive terms decreases by the aspect ratio α. In the far-field, we therefore have

$$i\omega\mu_0 j_0 E_s(\boldsymbol{x}') = k^2\int_V (N^2-1)\boldsymbol{E}\cdot\boldsymbol{e}^{(2)}E^p_{G2}dV \tag{20}$$

for the strength of the scattered field.

4. THE SCATTERED FIELD IN AND NEAR THE TARGET

We now formulate and solve a boundary value problem to construct the scattered near-field, in and near the target.

The magnetic field is eliminated from equations (4) by taking the curl of the first equation of the pair, to give

$$(\nabla^2+k^2N^2)\boldsymbol{E} = \nabla(\nabla\cdot\boldsymbol{E}). \tag{21}$$

The divergence of the second of equations (4) implies that $\nabla\cdot(N^2\boldsymbol{E}) = 0$, which can usefully be regarded as the expression for conservation of electric charge written in terms of $\boldsymbol{E}$. On expanding this relation and eliminating $\nabla\cdot\boldsymbol{E}$ from (21), we have

$$(\nabla^2+k^2N^2)\boldsymbol{E} = -\nabla\left(\frac{\boldsymbol{E}\cdot\nabla N^2}{N^2}\right). \tag{22}$$

Jump conditions across the target surface can be written in terms of $\boldsymbol{E}$ as

$$[\boldsymbol{E}\wedge\boldsymbol{n}] = 0\ \ [(\nabla\wedge\boldsymbol{E})\wedge\boldsymbol{n}] = 0\ \ [N^2\boldsymbol{E}\cdot\boldsymbol{n}] = 0\ \ \left[\frac{\nabla\cdot(N^2\boldsymbol{E})}{N^2}\right] = 0 \tag{23}$$

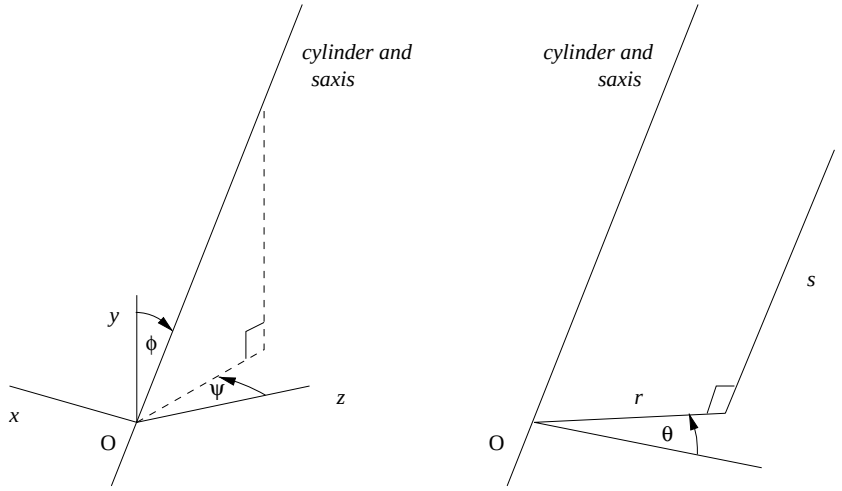

Figure 2. Target orientation and coordinate system: O' is an origin on the cylinder axis and the Cartesian $x'y'z'$-axes are parallel to the original xyz-axes of Figure 1. When the $x'y'z'$-axes are rotated through ϕ about $\boldsymbol{u} = \cos\psi \boldsymbol{e}^{(1)} - \sin\psi \boldsymbol{e}^{(3)}$, which is normal to the vertical plane containing the cylinder's axis, the y'-axis is rotated to the s-axis and the $y'z'$-coordinate plane is rotated to the $\theta = 0$ plane of the cylindrical coordinate system.

where $[\cdot]$ denotes the jump across the surface. The first two conditions follow from the curl equations (4), while the last two conditions follow from the expression $\nabla \cdot (N^2 \boldsymbol{E}) = 0$ noted below equation (21). These constitute six jump conditions for the sixth order system (22).

To construct the near-field solution, we introduce local cylindrical polar coordinates (r, θ, s) relative to an origin O' on the cylinder axis, which in turn has Cartesian coordinates (x_0, y_0, z_0) relative to the original coordinate system. The cylinder axis and s-axis coincide. The orientation of the cylinder axis is defined by introducing two angles, and we choose ϕ as the angle from the y-axis to the s-axis and ψ as the angle from the z-axis to the projection of the s-axis on the xz-coordinate plane, as indicated in Figure 2. The transformation from local polar to original Cartesian coordinates is

$$\begin{aligned} x &= x_0 + s\sin\psi\sin\phi + r(\sin\psi\cos\phi\cos(\theta-\psi) + \cos\psi\sin(\theta-\psi)) \\ y &= y_0 + s\cos\phi - r\sin\phi\cos(\theta-\psi) \\ z &= z_0 + s\cos\psi\sin\phi + r(\cos\psi\cos\phi\cos(\theta-\psi) - \sin\psi\sin(\theta-\psi)). \end{aligned} \tag{24}$$

We shall also need the expression for $\boldsymbol{e}^{(2)}$ in terms of unit vectors in

the polar coordinate directions, which is

$$\boldsymbol{e}^{(2)} = -\sin\phi\cos(\theta-\psi)\boldsymbol{e}^{(r)} + \sin\phi\sin(\theta-\psi)\boldsymbol{e}^{(\theta)} + \cos\phi\boldsymbol{e}^{(s)}, \quad (25)$$

and with the cylinder surface given by the equation $r = \rho(s)$ its outward normal $\boldsymbol{n}$ is in the direction $\boldsymbol{e}^{(r)} - \rho'(s)\boldsymbol{e}^{(s)}$. Here and elsewhere a prime on ρ is used to denote its derivative with respect to s.

The electric field is written as the sum of imposed and scattered contributions $\boldsymbol{E} = \boldsymbol{E}_i + \boldsymbol{E}_s$ as in (6). The imposed field satisfies equation (22) with N^2 set to unity everywhere, i.e., it satisfies the Helmholtz equation $(\nabla^2 + k^2)\boldsymbol{E}_i = 0$, and the scattered field is written in terms of its polar components $\boldsymbol{E}_s = (e_r, e_\theta, e_s)$. Inside the target N^2 is a function of the axial coordinate s alone and $\nabla N^2 = \partial_s N^2 \boldsymbol{e}^{(s)}$, so that setting $\boldsymbol{E}_i = E_i\boldsymbol{e}^{(2)}$ we find that $\boldsymbol{E}\cdot\nabla N^2 = (E_i\cos\phi + e_s)\partial_s N^2$. Equation (22) thus becomes

$$\begin{aligned}(\nabla^2 + k^2N^2)\boldsymbol{E}_s &= -k^2(N^2-1)E_i\boldsymbol{e}^{(2)} - \frac{\partial_s N^2}{N^2}\nabla_T(E_i\cos\phi + e_s) \\ &\quad -\boldsymbol{e}^{(s)}\frac{\partial}{\partial s}\left((E_i\cos\phi + e_s)\frac{\partial_s N^2}{N^2}\right)\end{aligned}$$

where ∇_T is the projection of ∇ on the $(r,\,\theta)$ plane.

In terms of the components of the scattered field, this is

$$Le_r - \frac{2}{r^2}\partial_\theta e_\theta + \frac{\partial_s N^2}{N^2}\partial_r e_s + (\partial_s^2 + k^2N^2)e_r =$$
$$k^2(N^2-1)E_i\sin\phi\cos(\theta-\psi) - \frac{\partial_s N^2}{N^2}\cos\phi\partial_r E_i \quad (26)$$
$$Le_\theta + \frac{2}{r^2}\partial_\theta e_r + \frac{\partial_s N^2}{N^2}\frac{1}{r}\partial_\theta e_s + (\partial_s^2 + k^2N^2)e_\theta =$$
$$-k^2(N^2-1)E_i\sin\phi\sin(\theta-\psi) - \frac{\partial_s N^2}{N^2}\frac{\cos\phi}{r}\partial_\theta E_i \quad (27)$$
$$\left(L + \frac{1}{r^2}\right)e_s + \partial_s\left(e_s\frac{\partial_s N^2}{N^2}\right) + (\partial_s^2 + k^2N^2)e_s =$$
$$-k^2(N^2-1)E_i\cos\phi - \cos\phi\partial_s\left(E_i\frac{\partial_s N^2}{N^2}\right) \quad (28)$$

where $L = \frac{1}{r}\partial_r r\partial_r - \frac{1}{r^2} + \frac{1}{r^2}\partial_\theta^2$. In terms of components, the jump conditions (23) are

$$[e_\theta] = 0 \quad [e_s] + \rho'[e_r] = 0 \quad [\partial_r e_s] - [\partial_s e_r] = 0 \quad [\partial_r e_\theta] - \frac{1}{\rho}[\partial_\theta e_r] = 0 \quad (29)$$

$$[N^2 e_r] - \rho'[N^2 e_s] = [N^2] E_i (\sin\phi \cos(\theta - \psi) + \rho' \cos\phi) \tag{30}$$

$$[\partial_r e_r] + \frac{1}{\rho}[e_r] + \left[\frac{\partial_s (N^2 e_s)}{N^2}\right] = -E_i \cos\phi \left[\frac{\partial_s N^2}{N^2}\right], \tag{31}$$

and are evaluated across $r = \rho(s)$. The last of conditions (29) follows on simplifying the θ component of the second of conditions (23), by noting that the quantities e_θ and $e_s + \rho' e_r$ are continuous across the cylinder surface and the derivatives ∂_θ and $\partial_s + \rho' \partial_r$ are tangential to the surface so that $[(\partial_s + \rho' \partial_r) e_\theta] = 0$ and $[\partial_\theta (e_s + \rho' e_r)] = 0$.

We construct the scattered near-field by a perturbation method based on the small aspect ratio of the cylindrical target. If ρ_0 is a reference value of the radius such as its average with respect to distance along the cylinder axis then $\rho_0 \ll W$ where W is the waveguide width, so that the aspect ratio is $\alpha = \frac{\rho_0}{W} \ll 1$. Inside and in the vicinity of the cylinder the scattered field varies on the length scale ρ_0 in the plane transverse to the cylinder axis but varies on the length scale W in the direction along the cylinder axis. It also depends parametrically on the aspect ratio. Thus

$$\boldsymbol{E}_s = \boldsymbol{E}_s(\frac{r}{\rho_0}, \theta, \frac{s}{W}; \alpha). \tag{32}$$

It follows that in the boundary value problem for the scattered field (26) to (31), $\frac{r}{s} \sim \alpha$ and when r and s derivatives act on the scattered field $\frac{\partial}{\partial r} \sim \frac{1}{\alpha}\frac{\partial}{\partial s}$. Also, since the cylinder radius $\rho(s)$ is of magnitude ρ_0 but varies on scale W, $\rho'(s) \sim \alpha$.

In contrast the imposed field is a smooth function of position everywhere and varies on the one length scale W in all directions, so that in local polar coordinates

$$\boldsymbol{E}_i = \boldsymbol{E}_i(\frac{r}{W}, \theta, \frac{s}{W}). \tag{33}$$

When r and s derivatives act on the imposed field $\frac{\partial}{\partial r} \sim \frac{\partial}{\partial s} \sim \frac{1}{W}$. Further, inside and in the vicinity of the target r is of order ρ_0, so that $\frac{r}{W} \sim \alpha$, and the imposed field and its derivatives are represented by their Taylor expansions in r, in which successive terms decrease in magnitude by a factor α. For example, the series for the imposed field $E_i = E_0 e_i$ is found from the expression for e_i in equations (2) and (3) under the transformation from Cartesian to polar coordinates (24) followed by expansion for small r. The first term in the series for e_i is written e_{i0}; it is a function of the axial coordinate s and the orientation angles ϕ and ψ, and is the imposed field evaluated on the target axis. Thus,

$$e_{i0} = e_i(x_0(s), z_0(s)) \qquad \text{where}$$

$$x_0(s) = x_0 + s\sin\psi\sin\phi \ \text{ and } \ z_0(s) = z_0 + s\cos\psi\sin\phi. \tag{34}$$

In view of the above remarks, inspection of the boundary value problem (26) to (31) shows that the components of the scattered field have expansions in terms of integer powers of α of the form

$$e_r = e_{r0} + e_{r1} + \ldots, \quad e_\theta = e_{\theta 0} + e_{\theta 1} + \ldots, \quad e_s = e_{s1} + \ldots, \tag{35}$$

where the subscript integer denotes the integer power of α that is the term's magnitude, e.g., $e_{r0} = O(1)$ and $e_{s1} = O(\alpha)$.

4.1. First Approximation to the Near-Field

The problem for the components of the scattered near-field in the first approximation, i.e., at order one with respect to α, is found by use of the expansion (35) in equations (26) and (27) with the first and fourth of jump conditions (29) and jump conditions (30) and (31). It is

$$Le_{r0} - \frac{2}{r^2}\partial_\theta e_{\theta 0} = 0 \quad Le_{\theta 0} + \frac{2}{r^2}\partial_\theta e_{r0} = 0 \tag{36}$$

subject to the jump conditions

$$[e_{\theta 0}] = 0 \quad [\partial_r e_{\theta 0}] - \frac{1}{\rho}[\partial_\theta e_{r0}] = 0 \tag{37}$$

$$[N^2 e_{r0}] = [N^2]E_0 e_{i0}\sin\phi\cos(\theta - \psi) \quad [\partial_r e_{r0}] + \frac{1}{\rho}[e_{r0}] = 0. \tag{38}$$

This has the solution

$$(e_{r0}, e_{\theta 0}) \ = \ \frac{N^2 - 1}{N^2 + 1}E_0 e_{i0}\sin\phi(\cos(\theta - \psi), -\sin(\theta - \psi)) \ \ 0 < r < \rho \tag{39}$$

$$(e_{r0}, e_{\theta 0}) \ = \ -\frac{N^2 - 1}{N^2 + 1}\frac{E_0 e_{i0}\rho^2}{r^2}\sin\phi(\cos(\theta - \psi), \ \sin(\theta - \psi)) \ \ \rho < r. \tag{40}$$

From this point on, when writing the solution for the scattered field for $r > \rho$ we use N^2 to denote its value taken at the same value of s but *inside* the target.

The mechanism that generates this leading order scattered field is expressed in the right-hand side of the first of the jump conditions (38), which is proportional to $\sin\phi$. In the absence of this term the system (36) to (38) would be homogeneous and e_{r0} and $e_{\theta 0}$ would vanish. When $\phi \neq 0$, the cylinder axis is out of complete alignment

with the direction of the imposed electric field, which therefore has a non-zero component in its transverse or (r, θ) plane. Free and loosely bound charges within the target material move in response to the imposed electric field, and the component in the transverse plane induces a periodic accumulation of charge at the target's surface over a microwave period. It is this surface charge which, in turn, induces the scattered field.

The scattered near-field constructed in equations (39) and (40) may lose validity near the end-points of the cylinder, where it intercepts the waveguide boundaries, for some choices of orientation. From the form (3) of the imposed field e_i for a TE_{10} guide, where the cylinder intercepts a sidewall $x = 0$ or $x = W$ or the short $z = L$ the factor e_{i0} in (39) and (40) vanishes on the cylinder axis but is non-zero and small like the cylinder radius ρ in a region that is confined to the near-field and within a distance of order ρ from the end. The scattered near-field (39) and (40) does not therefore satisfy exactly the boundary condition of zero tangential electric field on the sidewall over this small region, and is subject to an end-effect correction at higher order. However, where the cylinder intercepts a top or bottom waveguide boundary $y = 0$ or $y = H$, the factor e_{i0} is typically of order one, and unless the cylinder axis intercepts the boundary close to the normal so that the factor $\sin\phi \simeq 0$ in (39) and (40) the end-effect correction is of order one. Similarly, if the cylinder axis is parallel to a waveguide boundary and close to it on the order of the cylinder radius, the scattered near-field must be modified to account for the waveguide boundary conditions, and the correction is greatest when the axis is close to the boundaries $y = 0$ and $y = H$.

4.2. Second Approximation to the Near-Field

The second approximation to the scattered near-field, i.e., the field at order α, has longitudinal component e_{s1}, which satisfies the field equation

$$\left(L + \frac{1}{r^2}\right) e_{s1} \quad = \quad 0$$

and is subject to the jump conditions

$$[e_{s1}] + \rho'[e_{r0}] = 0 \qquad [\partial_r e_{s1}] - [\partial_s e_{r0}] = 0.$$

This problem is found by use of the expansion (35) in equation (28) and the second and third of jump conditions (29). It has the solution

$$e_{s1} = \begin{cases} \partial_s \left(\frac{N^2-1}{N^2+1} e_{i0} \right) r E_0 \sin\phi \cos(\theta - \psi) & 0 < r < \rho \\ \partial_s \left(\frac{N^2-1}{N^2+1} e_{i0} \rho^2 \right) \frac{E_0}{r} \sin\phi \cos(\theta - \psi) & \rho < r. \end{cases} \tag{41}$$

The r and θ components of the scattered near-field at order α satisfy the field equations

$$Le_{r1} - \frac{2}{r^2} \partial_\theta e_{\theta 1} = 0 \qquad Le_{\theta 1} + \frac{2}{r^2} \partial_\theta e_{r1} = 0$$

and are subject to the jump conditions

$$\begin{aligned} &[e_{\theta 1}] = 0 \quad [\partial_r e_{\theta 1}] - \frac{1}{\rho}[\partial_\theta e_{r1}] = 0 \\ &[N^2 e_{r1}] = [N^2] E_0 (e_{i1} \sin\phi \cos(\theta - \psi) + \rho' e_{i0} \cos\phi) \\ &[\partial_r e_{r1}] + \frac{1}{\rho}[e_{r1}] = -E_0 e_{i0} \left[\frac{\partial_s N^2}{N^2} \right] \cos\phi. \end{aligned} \tag{42}$$

These are found by pursuing expansion of the same equations that were used to formulate the leading order problem (36) to (38). Here e_{i1} is the second term in the Taylor expansion of e_i evaluated on the target surface $r = \rho(s)$. Since e_i is a function of the Cartesian coordinates x and z, we find from (24) that the term in jump condition (42) containing e_{i1} is

$$e_{i1} \sin\phi \cos(\theta - \psi) = \frac{\rho}{2} \sin\phi \{ \beta \cos\phi (1 + \cos 2(\theta - \psi)) + \gamma \sin 2(\theta - \psi) \}$$

where

$$\begin{pmatrix} \beta \\ \gamma \end{pmatrix} = \begin{pmatrix} \partial_x e_i & \partial_z e_i \\ -\partial_z e_i & \partial_x e_i \end{pmatrix}_{x_0(s), z_0(s)} \begin{pmatrix} \sin\psi \\ \cos\psi \end{pmatrix}.$$

Thus β and γ are functions of s, ϕ, and ψ.

The solution for e_{r1} and $e_{\theta 1}$ is the sum of θ-independent parts $(e_{r1}^{(0)}, e_{\theta 1}^{(0)})$ and θ-dependent parts $(e_{r1}^{(2)}, e_{\theta 1}^{(2)})$. The θ-independent part is

$$e_{r1}^{(0)} = \begin{cases} -E_0 e_{i0} \left(\frac{\partial_s N^2}{N^2} \right) \frac{r \cos\phi}{2} & 0 < r < \rho \\ -E_0 \left\{ e_{i0} \partial_s N^2 + (N^2 - 1) \left(\frac{2\rho'}{\rho} e_{i0} + \beta \sin\phi \right) \right\} \frac{\rho^2 \cos\phi}{2r} & \rho < r \end{cases} \tag{43}$$

with

$$e_{\theta 1}^{(0)} = 0 \quad \text{for all } r. \tag{44}$$

The θ-dependent part is

$$e_{r1}^{(2)} = \mathcal{E}_{r1} \begin{cases} r & 0 < r < \rho \\ \frac{-\rho^4}{r^3} & \rho < r \end{cases} \quad e_{\theta 1}^{(2)} = \mathcal{E}_{\theta 1} \begin{cases} r & 0 < r < \rho \\ \frac{\rho^4}{r^3} & \rho < r \end{cases} \tag{45}$$

where

$$\begin{pmatrix} \mathcal{E}_{r1} \\ \mathcal{E}_{\theta 1} \end{pmatrix} = \frac{N^2-1}{N^2+1}\frac{E_0}{2}\sin\phi \begin{pmatrix} \gamma & \beta\cos\phi \\ -\beta\cos\phi & \gamma \end{pmatrix} \begin{pmatrix} \sin 2(\theta-\psi) \\ \cos 2(\theta-\psi) \end{pmatrix}. \tag{46}$$

4.3. Power Deposition in the Target

The rate at which the electric field deposits energy within the target, averaged over a microwave period, has volume density $\frac{\sigma}{2}\boldsymbol{E}\cdot\boldsymbol{E}^*$. Averaging this over the target's circular cross-section, we have the average power density deposited within the target

$$< \mathcal{P} >= \frac{\sigma}{2\pi\rho^2}\int_{r<\rho} \boldsymbol{E}\cdot\boldsymbol{E}^* dA,$$

which is a function of the axial coordinate s.

The solution for the scattered near-field allows us to compute two successive approximations to $< \mathcal{P} >$. In the first approximation, the total electric field is given by

$$\boldsymbol{E} = E_0 e_{i0}\boldsymbol{e}^{(2)} + e_{r0}\boldsymbol{e}^{(r)} + e_{\theta 0}\boldsymbol{e}^{(\theta)},$$

where $(e_{r0}, e_{\theta 0})$ is the first approximation to the components of the scattered near-field inside the target as given by (39). Using this together with the expression (25) for $\boldsymbol{e}^{(2)}$ in a cylindrical geometry, we find that the average power over a cross-section is

$$< \mathcal{P} >= \frac{\sigma}{2}E_0^2|e_{i0}|^2 \left\{ 1 + \sin^2\phi \left(\left|\frac{N^2-1}{N^2+1}\right|^2 - 2\mathrm{Re}\left(\frac{N^2-1}{N^2+1}\right)\right)\right\}. \tag{47}$$

This can be regarded as a sum of three separate contributions, which can readily be identified on recalling that the first approximation to the scattered near-field (39) is proportional to $\frac{N^2-1}{N^2+1}$. Referring to the terms in parenthesis, the first contribution is the power deposition due to the imposed field alone, the second is due to the scattered field

alone, and the third is due to the superposition of both the imposed and scattered fields.

When the second approximation to the electric field is included, we find a non-zero correction to the power deposition at each point within the target. However, due to the azimuthal or θ-dependence of the first and second approximations to the total electric field, when this is averaged over the target cross-section we find that the correction to $< \mathcal{P} >$ which it induces is zero.

5. REFLECTION AND TRANSMISSION COEFFICIENTS FOR THE TARGET

We now evaluate the scattered electric field $\boldsymbol{E}_s$ far from the target and use it to derive expressions for the target's reflection and transmission coefficients. The scattered field is given by evaluating the integral in equation (20), for which we need the near-field solution of Section 4 and the far-field expansion of the Green's function (19).

Since the scattered far-field and the far-field Green's function are in the direction of the unit vector $\boldsymbol{e}^{(2)}$, we compute the quantity $\boldsymbol{E}\cdot\boldsymbol{e}^{(2)}$ in the integrand of (20), which has an expansion in terms of the target aspect ratio α. At leading order this is given by taking the expression (34) for the imposed field and the expression (39) for the scattered field inside the target. Using (25) for the expression of $\boldsymbol{e}^{(2)}$ in a cylindrical geometry, we have

$$\boldsymbol{E}\cdot\boldsymbol{e}^{(2)} = E_0 e_{i0}\left(1 - \frac{N^2-1}{N^2+1}\sin^2\phi\right) + O(\alpha). \tag{48}$$

Similarly, the arguments x and z of the far-field Green's function in the integrand of (20) are expanded with respect to r using the coordinate transformation (24).

Reflection

For reflection, the field point $\boldsymbol{x}'$ is to the left of the target, i.e., $z' < z$, so that from the comment immediately below equation (19), the far-field Green's function is a multiple of a left-going TE_{10} mode with argument $\boldsymbol{x}'$ and, on expansion for small r, the leading order imposed field e_{i0} evaluated on the target axis. On now interchanging $\boldsymbol{x}$ and $\boldsymbol{x}'$, we find that far from the target the scattered field is $\boldsymbol{E}_s = E_s\boldsymbol{e}^{(2)}$ where

$$E_s = \frac{i\pi k^2 E_0}{WHk_{10}}\sin\frac{\pi x}{W}e^{-ik_{10}z}\int_{s_1}^{s_2}\rho^2 e_{i0}^2(N^2-1)\left(1-\frac{N^2-1}{N^2+1}\sin^2\phi\right)ds. \tag{49}$$

The total electric field at a point far from the target is $\boldsymbol{E} = (E_0 e_i + E_s)\boldsymbol{e}^{(2)}$ in terms of the imposed and scattered fields, whereas in terms of the reflection coefficient R it is $\boldsymbol{E} = E_0 \sin\frac{\pi x}{W}(e^{ik_{10}z} + Re^{-ik_{10}z})\boldsymbol{e}^{(2)}$. Equating these two expressions and using (49) for the scattered field, we find that the reflection coefficient is

$$R = -e^{2ik_{10}L} + \frac{i\pi k^2}{WHk_{10}}\int_{s_1}^{s_2}\rho^2 e_{i0}^2(N^2-1)\left(1-\frac{N^2-1}{N^2+1}\sin^2\phi\right)ds \text{ with short.} \quad (50)$$

Here the first term is due to reflection from the short in the absence of the target and the second term is due to the presence of the target. In the absence of a short, we have what is formally the same as the last term in (50), i.e.,

$$R = \frac{i\pi k^2}{WHk_{10}}\int_{s_1}^{s_2}\rho^2 e_{i0}^2(N^2-1)\left(1-\frac{N^2-1}{N^2+1}\sin^2\phi\right)ds \text{ no short.} \quad (51)$$

In comparing these two expressions for R, we note that the scaled imposed field e_{i0} defined at (3) and (34) differs between (50) and (51).

Transmission

A transmission coefficient is defined only in the case where the waveguide has no short. For transmission, the field point $\boldsymbol{x}'$ of equation (20) is to the right of the target, so that the far-field Green's function is a multiple of a left-going TE_{10} mode with argument $\boldsymbol{x}$ and the imposed field e_i, which in this case of no short is a right-going TE_{10} wave, with argument $\boldsymbol{x}'$. On expanding the argument $\boldsymbol{x}$ for small r within the target and then interchanging $\boldsymbol{x}$ and $\boldsymbol{x}'$, we find that the scattered field far from the target is $\boldsymbol{E}_s = E_s\boldsymbol{e}^{(2)}$ where

$$E_s = \frac{i\pi k^2 E_0}{WHk_{10}}\sin\frac{\pi x}{W}e^{ik_{10}z}\int_{s_1}^{s_2}\rho^2|e_{i0}|^2(N^2-1)\left(1-\frac{N^2-1}{N^2+1}\sin^2\phi\right)ds. \quad (52)$$

In terms of the transmission coefficient T, the total electric field far to the right of the target is $\boldsymbol{E} = TE_0\sin\frac{\pi x}{W}e^{ik_{10}z}\boldsymbol{e}^{(2)}$. Equating this to the total electric field as the sum of the imposed and scattered fields, $\boldsymbol{E} = (E_0 e_i + E_s)\boldsymbol{e}^{(2)}$, we find from (52) that

$$T = 1 + \frac{i\pi k^2}{WHk_{10}}\int_{s_1}^{s_2}\rho^2|e_{i0}|^2(N^2-1)\left(1-\frac{N^2-1}{N^2+1}\sin^2\phi\right)ds \quad \text{no short.} \quad (53)$$

The absence of a short implies that $|e_{i0}|^2 = \sin^2 \frac{\pi x_0(s)}{W}$. It is useful to find an order of magnitude estimate for the reflection and transmission coefficients from the formulas (50), (51), and (53) by estimating the magnitude of the terms containing integrals over the length of the target axis within the guide. Each of these, which is necessarily dimensionless, contains a factor ρ^2 multiplied by a dimensional quantity that is of order $1/W^2$, so that the integral terms are all of order $O(\alpha^2)$, where $\alpha = \rho_0/W \ll 1$ is the target's aspect ratio.

We can proceed further. First, using the estimate for the electric field near the cylinder ends which was discussed after equations (39) and (40), we estimate the correction to the reflection and transmission coefficients due to end-effects. In the expression (20) for the scattered far-field, the region of integration over the cylinder ends is of order ρ^3. Where the cylinder intercepts a boundary $y = 0$ or $y = H$ the integrand in (20) is typically of order one, but where the cylinder intercepts a sidewall $x = 0$ or $x = W$ or the short $z = L$ since both the imposed field e_i and the Green's function (19) are of order ρ the integrand is of order ρ^2. The correction to the scattered far-field and the scattering coefficients that is caused by end-effects is therefore of order $O(\alpha^3)$ for an end that intercepts $y = 0$ or $y = H$ and is of order $O(\alpha^5)$ for an end that intercepts $x = 0$, $x = W$, or $z = L$. Next we compute the correction to the scattering coefficients due to the second approximation of the near-field away from the cylinder ends, which is given by (41) and (43) to (46). To do so, we compute the terms at order $O(\alpha)$ in equation (48) leaving a remainder at order $O(\alpha^2)$, and then compute the correction at order $O(\alpha^3)$ to the scattered far-field by evaluating the integral that appears in equation (20). However, in computing this integral, the azimuthal or θ-dependence of all terms for the correction is either $\sin(\theta - \psi)$ or $\cos(\theta - \psi)$ and integrates to zero over the target volume. As a result, the correction induced in the scattered far-field and the reflection and transmission coefficients is of order $O(\alpha^4)$. To each of the formulas (50), (51), and (53) we can therefore add an error bound that is at most of order $O(\alpha^3)$.

5.1. An Identity Satisfied by the Coefficients

A partial check on the validity of the expressions that have been derived for the target's reflection and transmission coefficients can be made as follows. The vector identity $\nabla \cdot (\boldsymbol{a} \wedge \boldsymbol{b}) = \boldsymbol{b} \cdot (\nabla \wedge \boldsymbol{a}) - \boldsymbol{a} \cdot (\nabla \wedge \boldsymbol{b})$ together with equations (4) and (5) show that

$$\nabla \cdot (\boldsymbol{E} \wedge \boldsymbol{H}^*) = iw(\mu_0 \boldsymbol{H} \cdot \boldsymbol{H}^* - \epsilon \boldsymbol{E} \cdot \boldsymbol{E}^*) - \sigma \boldsymbol{E} \cdot \boldsymbol{E}^*$$

where $*$ denotes the complex conjugate. The first two terms on the right-hand side are pure imaginary while the last term is real, so that on taking real parts we have

$$\mathrm{Re}\nabla \cdot (\boldsymbol{E} \wedge \boldsymbol{H}^*) = -\sigma \boldsymbol{E} \cdot \boldsymbol{E}^*.$$

When the last relation is integrated over a rectangular region of the waveguide, which is bounded by the waveguide sidewalls and two planes S_1 and S_2 at $z =$ constant to either side of the target, and the divergence theorem is used, we find the identity

$$-\mathrm{Re} \int_{S_1+S_2} (\boldsymbol{E} \wedge \boldsymbol{H}^*) \cdot \boldsymbol{n} dS = \int_V \sigma \boldsymbol{E} \cdot \boldsymbol{E}^* dV. \tag{54}$$

Here V denotes the volume of the target, outside which the conductivity σ vanishes, and $\boldsymbol{n}$ is the outward unit normal on the rectangular region of integration. The boundary conditions at a perfectly conducting surface have been used, i.e., that $\boldsymbol{E} \wedge \boldsymbol{n} = 0$ and $\boldsymbol{H} \cdot \boldsymbol{n} = 0$ so that $(\boldsymbol{E} \wedge \boldsymbol{H}^*) \cdot \boldsymbol{n} = 0$, to show that the surface integral over the guide sidewalls vanishes. Further, in the presence of a conducting short S_2 coincides with the short, and the surface integral in (54) is then over S_1 alone. The identity (54) has a simple physical interpretation, that, on multiplying through by one half, it equates the net electromagnetic energy flux irradiating the target, on the left-hand side, to the total power deposited within the target, on the right-hand side, time-averaged over the period of a microwave. The same result can be found by taking the time-average of Poynting's expression for conservation of electromagnetic energy.

To use the identity as a check on the expressions obtained for the reflection and transmission coefficients for the target, we note that its right-hand side can be expressed in terms of the time and cross-section averaged power deposition $< \mathcal{P} >$ of Section 4.3, as $2\pi \int_{s_1}^{s_2} \rho^2 < \mathcal{P} > ds$ where $s \in (s_1, s_2)$ denotes the axial length of the target within the waveguide, and that the expression for $< \mathcal{P} >$ valid to second order in the aspect ratio appears in equation (47). In the left-hand side of the identity, the plane S_1 with and without a short and the plane S_2 in the absence of a short are taken to be in the remote far-field of the target. The electric field strength there is expressed in terms of the reflection and transmission coefficients as defined above equations (50) and (53), and the magnetic field strength which is needed to compute the energy flux, is derived from the electric field using the first of equations (4).

Introducing the quantity

$$\mathcal{F}(N^2, \phi) = 1 + \sin^2 \phi \left(\left| \frac{N^2 - 1}{N^2 + 1} \right|^2 - 2\mathrm{Re} \left(\frac{N^2 - 1}{N^2 + 1} \right) \right),$$

which appears via the result (47) for $< \mathcal{P} >$, we find that the identity (54) gives the following relation to be satisfied by the absolute values of the coefficients, that

$$\frac{2\pi k^2}{k_{10} W H} \int_{s_1}^{s_2} \rho^2 |e_{i0}|^2 \mathrm{Im}(N^2) \mathcal{F}(N^2, \phi) ds + O(\alpha^3) = \begin{cases} 1 - |R|^2 - |T|^2 & \text{no short} \\ 1 - |R|^2 & \text{with short.} \end{cases} \tag{55}$$

The term containing the integral on the left-hand side is of order $O(\alpha^2)$, and the error bound $O(\alpha^3)$ follows from the remarks below equation (53) concerning correction to the scattered field due to end-effects.

It is now a matter of straightforward algebraic manipulation to verify that the formulas given for the reflection and transmission coefficients at (50), (51), and (53) satisfy the relation (55).

5.2. Examples

We consider specific examples for a cylindrical target of constant radius 0.4 cm that is placed in a TE_{10} waveguide with short, a microwave source of frequency 2.45 GHz, and standard waveguide width $W = 8.64$ cm and height $H = 4.32$ cm. The quantity we calculate is $R_t = R + e^{2ik_{10}L}$, where R is the reflection coefficient of equation (50) for the target and short, so that R_t is given by evaluation of the integral in (50) and is the contribution to R due to the target alone.

We consider two locations of the origin $O'(x_0, y_0, z_0)$ on the target axis, with respect to which the orientation angles ϕ and ψ and positions of the short $z = L$ are taken, see Figures 1 and 2. These are referred to as

$$\begin{aligned} &\text{location 1: } x_0 = W/2,\ y_0 = H/2,\ z_0 = 0,\ L = \pi/(2k_{10}), \\ &\text{location 2: } x_0 = W/3,\ y_0 = H/2,\ z_0 = 0,\ L = \pi/(3k_{10}). \end{aligned}$$

Location 1 is at a local maximum of the imposed electric field strength, while location 2 is slightly removed from it being closer to one side of the waveguide and closer to the short. A constant baseline profile of

$$N^2 = N_0^2 = 10 + i0.00073$$

is taken based on data for alumina at 2.45 GHz and uniform temperature 30°C [9]. To indicate the effect of an inhomogeneity in the target's electrical conductivity we also consider a modified profile of

$$N^2 = N_m^2 = N_0^2 + i0.073 \exp\left(-\frac{(s-1)^2}{2}\right)$$

Table 1. Values of $\mathrm{Re}(R_t)$ and $\mathrm{Im}(R_t)$ for a cylinder placed vertically at two different locations in a waveguide with short. N^2 is either constant (N_0^2) or modified by a Gaussian spike in electrical conductivity (N_m^2).

Location: (x_0, L)	N^2	$\mathrm{Re}(R_t)$	$\mathrm{Im}(R_t)$
1: $(W/2, \pi/2k_{10})$	constant, N_0^2	-0.00012354	1.52309344
1: $(W/2, \pi/2k_{10})$	Gaussian, N_m^2	-0.00640426	1.52309344
2: $(W/3, \pi/3k_{10})$	constant, N_0^2	0.74192391	0.42843021
2: $(W/3, \pi/3k_{10})$	Gaussian, N_m^2	0.74015746	0.43148980

which has a Gaussian 'spike' in the conductivity of 100 times the baseline value centered 1 cm from the origin with length scale $\sqrt{2}$ cm. This increase in conductivity corresponds to a localized temperature increase to 1400^oC at the spike center for alumina, and values for silica under the same conditions are very nearly the same [9].

The real and imaginary parts of R_t for a vertical orientation of the cylinder's axis, $\phi = 0$, are given in Table 1. With this orientation the imposed electric field strength is constant along the cylinder axis, and with $N^2 = N_0^2$ a change from location 1 to location 2 decreases the modulus of R_t by a factor of 9/16 and decreases its argument by $\pi/3$. The change in R_t that is caused by change of the conductivity profile from the constant N_0^2 to Gaussian N_m^2 profile with location fixed is small, at most 2% in $\mathrm{Re}(R_t)$.

In Figure 3 we show the real and imaginary parts of R_t for the target with $N^2 = N_0^2$, origin at location 1, and constant angle of declination $\phi = 2\pi/7$ for $\psi \in [0, 2\pi]$. Here, ϕ is sufficiently small that for all ψ the ends of the cylindrical target intercept the top and bottom sides, $y = 0$ and $y = H$, of the waveguide and with the symmetrical location of the target origin there is a high degree of symmetry to this configuration. The plot in the R_t plane shows a straight line, and points are marked on the path for $\psi = 0$ near bottom right end, $\psi = \pi/4$ at top left end, and $\psi = \pi/2$ at bottom right end. The same path is traced out continuously with further increase of ψ. Figure 4 shows the effect of change to the Gaussian profile $N^2 = N_m^2$ on R_t with all other conditions the same. The path in the R_t plane splits due to the presence of the inhomogeneity, and from the different scales of the real axes in the two figures a significant change in $\mathrm{Re}(R_t)$ is seen with a much smaller change in $\mathrm{Im}(R_t)$. Figure 5 shows $\mathrm{Im}(R_t)$ versus $\psi/2\pi$ for the conditions of Figure 4 from which R_t is seen to be an even function of ψ about $\psi = \pi/2$ and $\psi = \pi$.

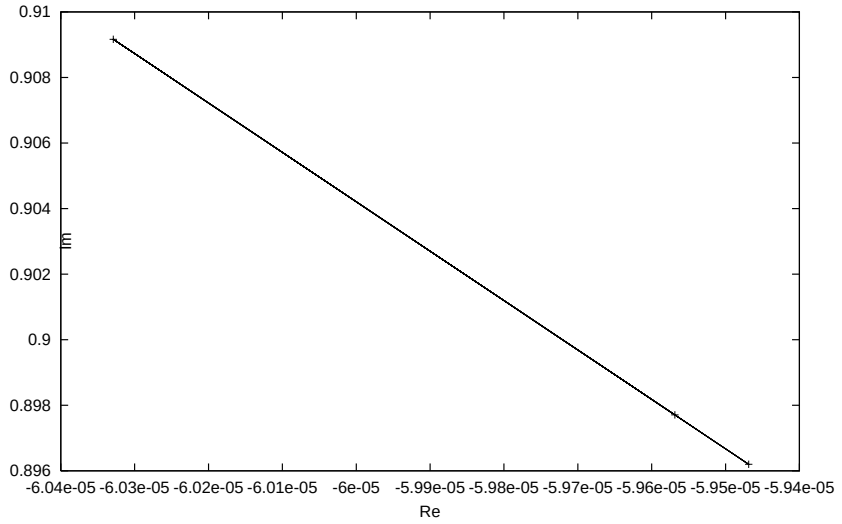

Figure 3. Real and Imaginary parts of R_t for $N^2 = N_0^2$, location 1, $\phi = 2\pi/7$, and $\psi \in [0, 2\pi]$.

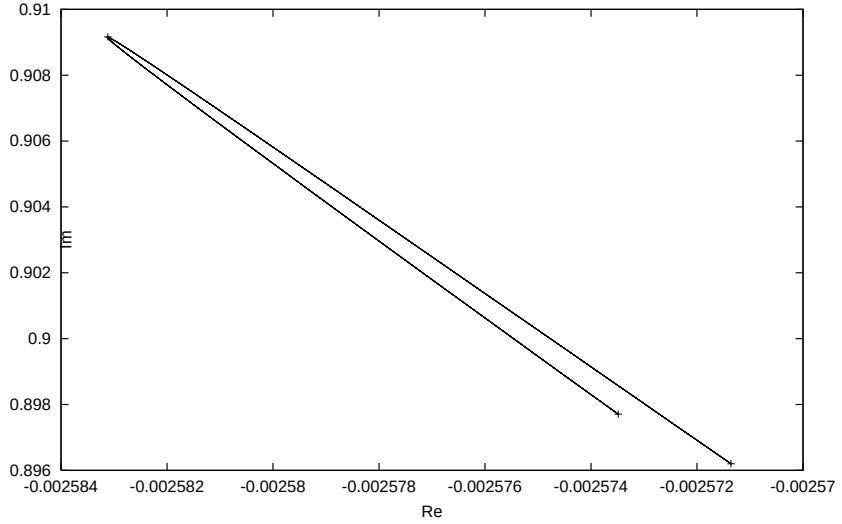

Figure 4. Real and Imaginary parts of R_t for the same conditions as in figure 3 but with $N^2 = N_m^2$.

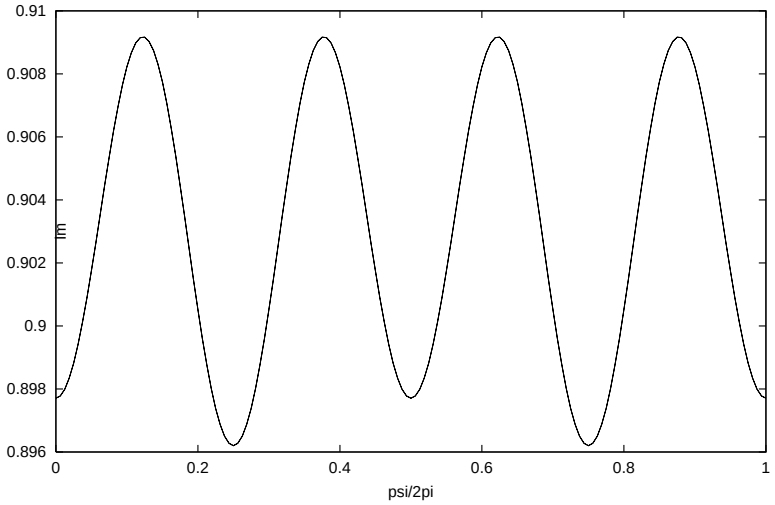

Figure 5. $\mathrm{Im}(R_t)$ versus $\psi/2\pi$ for the same conditions as in figure 4

Next we consider the effect of increasing the angle of declination of the cylinder's axis to $\phi = 3\pi/7$ with the origin at the same location 1. Now ϕ is sufficiently large that when $\psi = 0$ one end of the axis intercepts the waveguide short $z = L$, while the other end intercepts the bottom side $y = 0$. As ψ is increased to $\psi_{c1} \simeq 0.1509\pi$ this end intercepts the side $x = 0$ and with further increase of ψ past $\psi_{c2} \simeq 0.2496\pi$ the end that intercepted the short begins to intercept the side $x = W$. The real and imaginary parts of R_t with constant $N^2 = N_0^2$ are given in Figure 6 for $\psi \in [0, 2\pi]$, which shows a straight line. The path is traced out from the top left of the figure when $\psi = 0$ to the bottom right when $\psi = \pi/2$ but in a non-monotone way; as ψ is increased from a value that is just greater than ψ_{c1} to a value equal to ψ_{c2} the direction of the path in the R_t plane is reversed and values of R_t at these values of ψ are indicated in the figure by points. The path is traced out continuously as ψ is increased further.

Figure 7 shows the effect of change to the Gaussian profile $N^2 = N_m^2$ on R_t with all other conditions as in Figure 6. Figure 7 shows a substantial change in the shape of the path in the R_t plane, which is due mostly to a change in the magnitude and behavior of $\mathrm{Re}(R_t)$. The path is traced out from the top left when $\psi = 0$ to the bottom right when $\psi = \pi/2$, and has a turning point when ψ is just less than ψ_{c1} and a cusp at $\psi = \psi_{c2}$. The combination of a value of ϕ that is sufficiently large that the ends of the cylinder can intercept the short with the displacement of the inhomogeneity in electrical conductivity

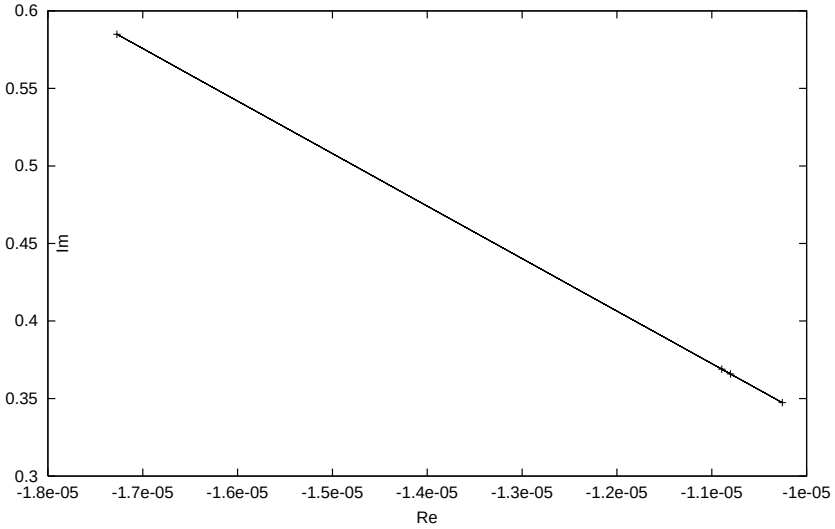

Figure 6. Real and Imaginary parts of R_t for $N^2 = N_0^2$, location 1, increased declination $\phi = 3\pi/7$, and $\psi \in [0, 2\pi]$.

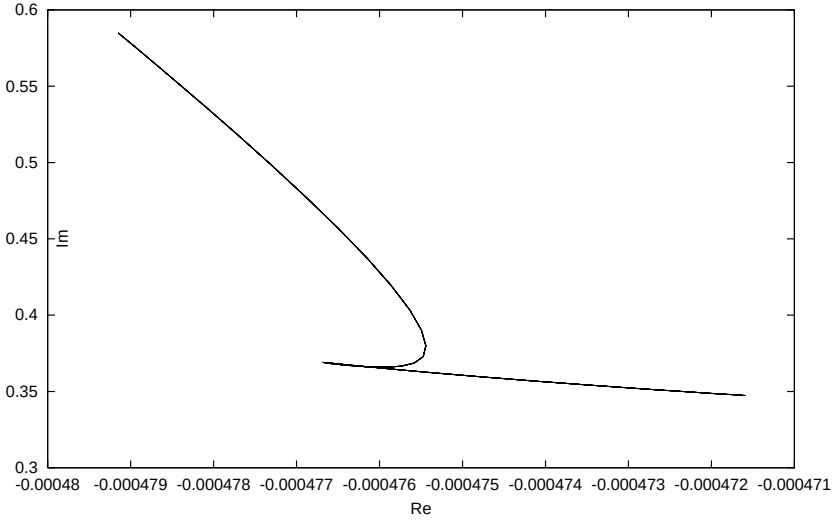

Figure 7. Real and Imaginary parts of R_t for the same conditions as in figure 6 but with $N^2 = N_m^2$.

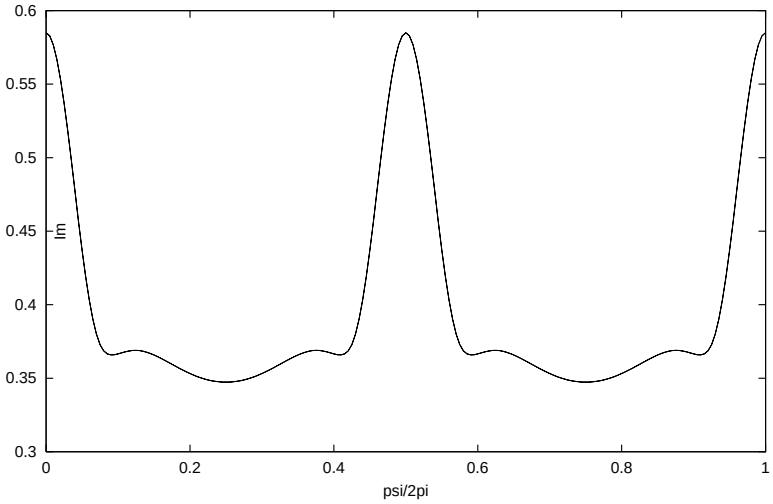

Figure 8. $\mathrm{Im}(R_t)$ versus $\psi/2\pi$ for the conditions of figure 7.

away from the origin O' introduces an asymmetry to R_t about $\psi = \pi/2$, but this effect is found to be numerically small. When ψ is increased beyond $\pi/2$ the path in the R_t plane is retraced exactly until the cusp is reached at $\psi = \pi - \psi_{c2}$. With further increase of ψ the initial path of R_t is followed so closely that departure from it is not visible on the scale of the figure, being at most in the ninth decimal place in $\mathrm{Re}(R_t)$ and always less than the tenth decimal place in $\mathrm{Im}(R_t)$. Figure 8 shows $\mathrm{Im}(R_t)$ versus $\psi/2\pi$ for this case, from which much of the change in R_t is seen to occur when ψ is close to either zero or π.

When the cylinder origin O' is moved to location 2, closer to the waveguide short and sidewall $x = 0$, the electric field intensity is reduced over much of its length. For a given orientation of the cylinder's axis the effect of a change in N^2 from constant N_0^2 to modified N_m^2 is therefore expected to be less than that found for location 1. Figure 9 shows the path traced out in the R_t plane for location 2 with declination $\phi = 2\pi/7$ for $\psi \in [0, 2\pi]$. This shows a straight line (dashed) for constant $N^2 = N_0^2$ and the curve nearby for non-constant $N^2 = N_m^2$. Although the difference in R_t that is caused by the change in N^2 is confirmed to be slight, its effect is sufficient to show a just-perceptible change in the path from a straight line to form a narrow V-shape. When the declination is increased further to $\phi = 3\pi/7$ this difference, though still present, is too small to be visible in a figure, and the difference in the real and imaginary parts of R_t at a given value of ψ is less than 0.25%.

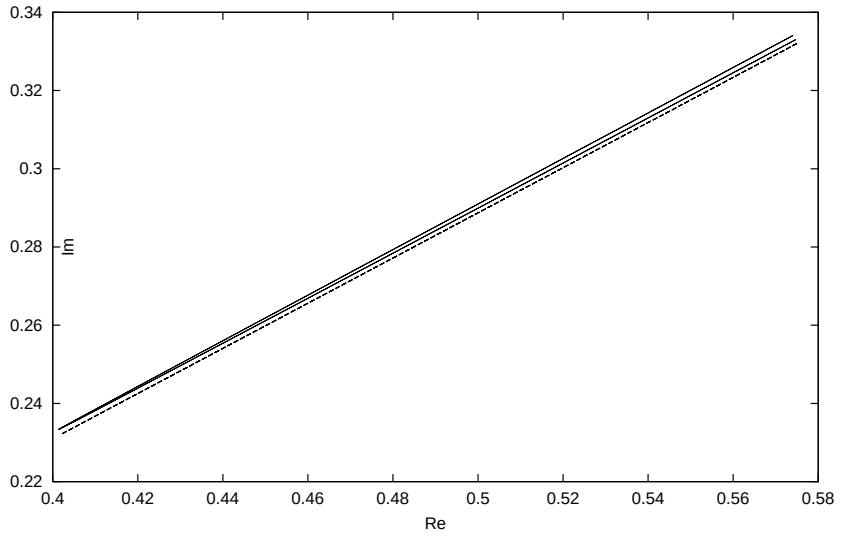

Figure 9. Real and Imaginary parts of R_t for $N^2 = N_0^2$ (dashed) and $N^2 = N_m^2$ (solid line), location 2, $\phi = 2\pi/7$, and $\psi \in [0, 2\pi]$.

6. CONCLUSION

We have used a dyadic Green's function technique to derive reflection and transmission coefficients for a narrow, inhomogeneous cylindrical target that has arbitrary orientation in a rectangular TE_{10} waveguide. The technique gives the scattered far-field in terms of the total electric field within the target, which in turn is constructed by solving the problem for the scattered field in and near the target by a multiple scales perturbation method.

The multiple scales method is based on the target's small aspect ratio. That is, as a function of distance, the scattered near-field varies on the length scale of the target's radius in the plane perpendicular to the target's axis, while it varies on the length scale of the waveguide width in the direction parallel to the target's axis. Conversely, since they are independent of the presence of a target within the guide, both the imposed electric field and the Green's function vary solely on the length scale of the waveguide width.

The solution for the scattered near-field has been used to derive an expression (47) for the power deposition or rate of generation of heat inside the target, averaged over its narrow cross-section and the fast time scale of a microwave period. This expression will appear as a source term in an equation for the target's thermal energy balance,

which can be solved to find its temperature provided the temperature-dependence of the electrical conductivity is known.

An expression for the reflection coefficient of the target when the waveguide has a perfectly conducting short has been given at (50), and expressions for the reflection and transmission coefficients in the absence of a short have been given at (51) and (53). Each of these expressions, which are dimensionless, shows that the contribution of the target alone to the reflected and transmitted far-fields is of order $O(\alpha^2)$, where $\alpha \ll 1$ is the target's aspect ratio. By constructing the first correction to the scattered field within the target for small α and considering end-effects, we have shown that the expressions given for the reflection and transmission coefficients have an error that is at most of order $O(\alpha^3)$.

The analysis has been carried out for a general, inhomogeneous target, for which the target material's electrical properties, its permittivity and electrical conductivity, are arbitrary functions of position along the target's axis. As explained in the Introduction, this generalization is necessary when the material's electrical properties, and in particular its electrical conductivity, are temperature dependent and the target is subjected to an imposed field that has a spatial gradient and is of a sufficient intensity that it heats the target. This situation typically occurs in microwave heating applications, where a target may reach temperatures of 1400°C or more.

Our motivation for considering the scattering problem has been two-fold. First, in a low intensity field the target is very nearly homogeneous and its electrical properties can be determined in terms of the one dimensionless grouping N^2 by measuring the strength of the scattered field and using the expressions that have been given for the reflection and transmission coefficients. Second, in microwave heating applications the target is often placed in a resonant cavity between an iris or diaphragm and a short, and the cavity is tuned by varying its length and aperture width so as to significantly increase the imposed field. If the target is sufficiently removed from the iris that evanescent mode interaction can be neglected, S-matrix theory can be applied as in [10] to combine expressions for the scattering coefficients for an isolated iris and a target with short to determine parameters that optimize the field within the cavity and enhance the heating process.

We have included the effect of variations in the cylindrical target's radius that are on the length scale of the waveguide width. This effect is absent from the expression for the averaged power deposition but does appear in the expressions for the target's scattering coefficients and will appear in the energy balance for the target's temperature.

The analysis is restricted to values of $\mathrm{Im}(N^2)$ that are small or of

order one in magnitude. For a highly conducting target, $\mathrm{Im}(N^2)$ can be sufficiently large that the skin depth δ is smaller than the target radius, and δ then enters the problem as an additional length scale for the scattered near-field. Although the multiple scales analysis of Section 4 could be extended to include such a case, microwaves do not provide an effective means of heating a target in the high conductivity limit. Further, for ceramics, the electrical conductivity data of [9] indicates a value of the skin depth $\delta \simeq 3.25\,\mathrm{cm}$ for alumina at $4\,\mathrm{GHz}$ and $1400°\mathrm{C}$, while at lower frequencies and temperatures δ is still larger. Values of δ in the centimeter range are of the same order of magnitude as the waveguide width, as opposed to being the same or smaller than the values of a high aspect ratio target's radius, which is of the order of millimeters or less. The electrical conductivity can increase by a further two orders of magnitude before δ decreases toward the millimeter range.

APPENDIX A. THE DYADIC GREEN'S FUNCTION

When $i = 2$ the divergence of equation (10) implies that $\nabla.\boldsymbol{E}_{G2} = -i\kappa\partial_y\delta(\boldsymbol{x}-\boldsymbol{x}')$ where $\kappa = \frac{j_0}{\omega\epsilon_0}$, so that equation (11) can be written

$$(\nabla^2 + k^2)\boldsymbol{E}_{G2} = -i\kappa\left(\partial^2_{xy}\boldsymbol{e}^{(1)} + (\partial^2_{yy} + k^2)\boldsymbol{e}^{(2)} + \partial^2_{yz}\boldsymbol{e}^{(3)}\right)\delta(\boldsymbol{x}-\boldsymbol{x}').$$

The boundary conditions on the sidewalls, and on the short if present, are given by (13)

$$\boldsymbol{E}_{G2}\wedge\boldsymbol{n} = 0 \quad \text{and} \quad \frac{\partial}{\partial n}(\boldsymbol{E}_{G2}.\boldsymbol{n}) = 0.$$

A condition of no incoming radiation is imposed as $z \to -\infty$, and in the absence of a short as $z \to \infty$. We construct the Cartesian components E_{Gi} of $\boldsymbol{E}_{G2}$. The problem for the x-component is

$$(\nabla^2 + k^2)E_{G1} = -i\kappa\delta'(x-x')\delta'(y-y')\delta(z-z')$$

$$\text{on } x = 0, W \;\; \partial_x E_{G1} = 0, \quad \text{on } y = 0, H \;\; E_{G1} = 0$$

$$\text{and, with a short, on } z = L \;\; E_{G1} = 0$$

The transverse eigenfunctions are therefore

$$\phi_{mn} = \begin{cases} \sqrt{\frac{2}{WH}}\sin\frac{n\pi y}{H} & m = 0,\ n = 1, 2, \ldots \\ \frac{2}{\sqrt{WH}}\cos\frac{m\pi x}{W}\sin\frac{n\pi y}{H} & m, n = 1, 2, \ldots \end{cases} \tag{A1}$$

Setting $E_{G1} = \sum_{m,n} \alpha_{mn}\phi_{mn}$, we find that α_{mn} satisfies

$$(\partial_z^2 + k_{mn}^2)\alpha_{mn} = -i\kappa\partial_{x'y'}^2\phi_{mn}(x', y')\delta(z - z') \tag{A2}$$

where

$$k_{mn}^2 = k^2 - \left(\left(\frac{m\pi}{W}\right)^2 + \left(\frac{n\pi}{H}\right)^2\right). \tag{A3}$$

This expression for k_{mn} is the same as the expression for the z component of the wavenumber of TE and TM modes in the waveguide. For a TE_{10} waveguide $\frac{\pi}{W} < k < \min(\frac{\pi}{H}, \frac{2\pi}{W})$, so that $k_{mn}^2 > 0$ if and only if $m = 1$ and $n = 0$; this is the only mode that propagates in the z direction and all other modes are evanescent. Here, the transverse eigenfunctions ϕ_{mn} have indices $m = 0, 1, \ldots$ and $n = 1, 2, \ldots$ so that there is no term with $m = 1$ and $n = 0$ in the sum. As a result, all terms in the sum for E_{G1} are evanescent, and from the expression (20) for the magnitude of the scattered field, the x component of the Green's function does not contribute to the scattered field far from the target.

When $m = 0$, ϕ_{mn} is independent of x and the right-hand side of equation (A2) is zero, so that $\alpha_{0n} = 0$ and the index range in the sum is thus restricted further to $m, n = 1, 2, \ldots$. For later reference, it is useful to give the expression for the x component of the Green's function, which is

$$E_{G1} = -\frac{\kappa}{2}\sum_{m,n=1}^{\infty}\frac{1}{k_{mn}}\phi_{mn}(x, y)\partial_{x'y'}^2\phi_{mn}(x', y')\psi_{mn}(z, z')$$

$$\text{where } \psi_{mn} = \begin{cases} e^{ik_{mn}|z-z'|} & \text{no short} \\ e^{ik_{mn}|z-z'|} - e^{-ik_{mn}(z+z'-2L)} & \text{with short.} \end{cases} \tag{A4}$$

For the y-component, the problem is

$$(\nabla^2 + k^2)E_{G2} = -i\kappa\delta(x - x')(\delta''(y - y') + k^2\delta(y - y'))\delta(z - z')$$

$$\text{on } x = 0, W \;\; E_{G2} = 0, \quad \text{on } y = 0, H \;\; \partial_y E_{G2} = 0$$

$$\text{and, with a short, on } z = L \;\; E_{G2} = 0.$$

The transverse eigenfunctions can be formed from (A1) by interchanging both m and n and the dimensionless coordinates x/W and y/H, so that if the same symbol ϕ_{mn} is used, here

$$\phi_{mn} = \begin{cases} \sqrt{\frac{2}{WH}}\sin\frac{m\pi x}{W} & n = 0, \; m = 1, 2, \ldots \\ \frac{2}{\sqrt{WH}}\sin\frac{m\pi x}{W}\cos\frac{n\pi y}{H} & m, n = 1, 2, \ldots \; . \end{cases} \tag{A5}$$

and the index set is now $m = 1, 2, \ldots$ and $n = 0, 1, \ldots$. With $E_{G2} = \sum_{m,n} \alpha_{mn}\phi_{mn}$, the coefficients α_{mn} satisfy

$$(\partial_z^2 + k_{mn}^2)\alpha_{mn} = -i\kappa(\partial_{y'}^2 + k^2)\phi_{mn}(x', y')\delta(z - z'), \tag{A6}$$

which is equation (A2) under $\partial_{x'y'}^2\phi_{mn} \mapsto (\partial_{y'}^2 + k^2)\phi_{mn}$.

The transverse eigenfunctions for E_{G2} now include the one propagating $m = 1$ and $n = 0$ mode among the index set $m = 1, 2, \ldots$ and $n = 0, 1, \ldots$. Further, the right-hand side of equation (A6) and hence the coefficients α_{mn} are non-zero for all such m and n. The expression for E_{G2} is therefore given from (A4) by modifying the index set and putting $\partial_{x'y'}^2\phi_{mn} \mapsto (\partial_{y'}^2 + k^2)\phi_{mn}$, so that

$$E_{G2} = -\frac{\kappa}{2} \sum_{(m,\,n)=(1,\,0)}^{\infty} \frac{1}{k_{mn}} \phi_{mn}(x,\, y)(\partial_{y'}^2 + k^2)\phi_{mn}(x',\, y')\psi_{mn}(z,\, z') \tag{A7}$$

where ϕ_{mn} is defined by (A5) but ψ_{mn} remains unchanged from (A4).

The problem for the z-component of the Green's function is

$$(\nabla^2 + k^2)E_{G3} = -i\kappa\delta(x - x')\delta'(y - y')\delta'(z - z')$$

$$\text{on } x = 0, W \;\; E_{G3} = 0, \quad \text{on } y = 0, H \;\; E_{G3} = 0$$

$$\text{and, with a short, on } z = L \;\; \partial_z E_{G3} = 0.$$

The transverse eigenfunctions are

$$\phi_{mn} = \frac{2}{\sqrt{WH}} \sin\frac{m\pi x}{W} \sin\frac{n\pi y}{H} \quad m,\, n = 1,\, 2, \ldots,$$

and with $E_{G3} = \sum_{m,n} \alpha_{mn}\phi_{mn}$ the α_{mn} satisfy

$$(\partial_z^2 + k_{mn}^2)\alpha_{mn} = i\kappa\partial_{y'}\phi_{mn}(x',\, y')\delta'(z - z').$$

The one propagating $m = 1$ and $n = 0$ mode is not included in the index set, so that by the same reasoning given after equation (A3) for the x-component the Green's function, each term in the sum for the z-component is evanescent and neither component of the Green's function contributes to the scattered field far from the target. For completeness, we give the expression

$$E_{G3} = \frac{i\kappa}{2} \sum_{m,\,n=1}^{\infty} \phi_{mn}(x, y)\partial_{y'}\phi_{mn}(x', y')\psi_{mn}(z, z')$$

$$\text{where } \psi_{mn} = \begin{cases} \partial_z|z - z'|e^{ik_{mn}|z-z'|} & \text{no short} \\ \partial_z|z - z'|e^{ik_{mn}|z-z'|} - e^{-ik_{mn}(z+z'-2L)} & \text{with short.} \end{cases}$$

We see that only the y-component of the Green's function contributes to the scattered field far from the target, and the contribution is given by taking the one term with $m = 1$ and $n = 0$ in the sum of (A7). This is the far-field approximation of the Green's function, $\boldsymbol{E}_{G2} \sim E^p_{G2}\boldsymbol{e}^{(2)}$ where

$$E^p_{G2}(\boldsymbol{x}, \boldsymbol{x}') = \frac{-j_0 k^2}{\omega\epsilon_0 WHk_{10}} \sin\frac{\pi x}{W} \sin\frac{\pi x'}{W} \begin{cases} e^{ik_{10}|z-z'|} & \text{no short} \\ e^{ik_{10}|z-z'|} - e^{-ik_{10}(z+z'-2L)} & \text{with short.} \end{cases} \tag{A8}$$

REFERENCES

1. Lewin, L., *Theory of Waveguides*, J. Wiley and Sons, New York, 1975.
2. Leviatan, Y. and G. S. Sheaffer, "Analysis of inductive dielectric posts in rectangular waveguide," *IEEE Trans. Microwave Theory and Techniques*, Vol. 35, No. 1, 48–59, 1987.
3. Gesche, R. and N. Lochel, "Scattering by a lossy dielectric cylinder in a rectangular waveguide," *IEEE Trans. Microwave Theory and Techniques*, Vol. 36, No. 1, 137–144, 1988.
4. Siakavara, S. and J. N. Sahalos, "The discontinuity problem of a rectangular dielectric post in a rectangular waveguide," *IEEE Trans. Microwave Theory and Techniques*, Vol. 39, No. 9, 1617–1622, 1991.
5. Abdulnour, J. and L. Marchildon, "Scattering by a dielectric obstacle in a rectangular waveguide," *IEEE Trans. Microwave Theory and Techniques*, Vol. 41, No. 11, 1988–1994, 1993.
6. Chumachenko, V. P., S. I. Tarapov, and S. Eker, "Scattering by a lossy dielectric cylinder in a waveguide cross-junction," *IEE Proc. Microw. Antennas Propag.*, Vol. 149, No. 4, 229–236, 2002.
7. Jones, D. S., *Acoustic and Electromagnetic Waves*, Oxford University Press, 1986.
8. Kevorkian, J. and J. D. Cole, *Multiple Scale and Singular Perturbation Methods*, Springer Verlag, New York, 1996.
9. Westphal, W. B., "Dielectric constant and loss measurements in high-temperature materials," Laboratory for Insulation Research, MIT, Cambridge, Massachusetts, 1963.
10. Kriegsmann, G. A., "Hot spot formation in microwave heated ceramic fibres," *IMA Journal of Applied Mathematics*, Vol. 59, 123–148, 1997.
11. Kriegsmann, G. A., "Pattern formation in microwave heated ce-

ramics: cylinders and slabs," *IMA Journal of Applied Mathematics*, Vol. 66, No. 1, 1–32, 2001.

12. Stratton, J. A., *Electromagnetic Theory*, McGraw-Hill Book Company, New York, 1941.

Michael R. Booty received the M.A. degree in mathematics from the University of Cambridge in 1979, and the Ph.D. degree in mathematics from Imperial College London in 1983. He was a SERC research fellow from 1982 to 1984, and a postdoctoral fellow at Northwestern University from 1984 to 1987. He is currently Associate Professor of Mathematical Sciences at New Jersey Institute of Technology. His research interests include asymptotic methods, mathematical modeling and wave propagation.

Gregory A. Kriegsmann received the M.S. degree in electrical engineering and the Ph.D. degree in applied mathematics from the University of California, Los Angeles, in 1970 and 1974, respectively. He was a Courant Instructor in Applied Mathematics at New York University from 1974 to 1976, and an Associate and Full Professor of Applied Mathematics at Northwestern University from 1980 to 1990. He is currently Professor of Mathematical Sciences and Foundation Chair of Applied Mathematics at the New Jersey Institute of Technology. His research interests include the development of asymptotic and numerical methods for solving wave propagation and scattering problems.